Hybrid Polymer/Zinc Oxide Photovoltaic Devices with Vertically Oriented ZnO Nanorods and an Amphiphilic Molecular Interface Layer

Punniamoorthy Ravirajan,[†,‡] Ana M. Peiró,[§] Mohammad K. Nazeeruddin,[⊥] Michael Graetzel,[⊥] Donal D. C. Bradley,[†] James R. Durrant,[§] and Jenny Nelson*[,†]

Department of Physics, Imperial College London, Prince Consort Road, London SW7 2BW, United Kingdom, Centre for Electronic Materials and Devices, Department of Chemistry, Imperial College London, London SW7 2AZ, United Kingdom, Institute of Molecular and Biological Chemistry, Faculty of Basic Science, École Polytechnique Fédérale de Lausanne, Lausanne, Switzerland, and Department of Physics, University of Jaffna, Jaffna, Sri Lanka

Received: December 7, 2005; In Final Form: February 27, 2006

We report on the effect of nanoparticle morphology and interfacial modification on the performance of hybrid polymer/zinc oxide photovoltaic devices. We compare structures consisting of poly-3-hexylthiophene (P3HT) polymer in contact with three different types of ZnO layer: a flat ZnO backing layer alone; vertically aligned ZnO nanorods on a ZnO backing layer; and ZnO nanoparticles on a ZnO backing layer. We use scanning electron microscopy, steady state and transient absorption spectroscopies, and photovoltaic device measurements to study the morphology, charge separation, recombination behavior and device performance of the three types of structures. We find that charge recombination in the structures containing vertically aligned ZnO nanorods is remarkably slow, with a half-life of several milliseconds, over 2 orders of magnitude slower than that for randomly oriented ZnO nanoparticles. A photovoltaic device based on the nanorod structure that has been treated with an amphiphilic dye before deposition of the P3HT polymer yields a power conversion efficiency over four times greater than that for a similar device based on the nanoparticle structure. The best ZnO nanorod:P3HT device yields a short circuit current density of 2 $mAcm^{-2}$ under AM1.5 illumination (100 mW cm^{-2}) and a peak external quantum efficiency over 14%, resulting in a power conversion efficiency of 0.20%.

Introduction

Nanostructured composite materials containing an electron-accepting component and an electron-donating component in a "bulk heterojunction" structure are promising systems for photovoltaic energy conversion with organic semiconductors. The highest reported efficiencies have been for blends of conjugated polymers or molecules as the donor with fullerenes as the electron acceptor.[1] However, the difficulty of controlling the morphology of the blend and the tendency toward phase segregation over time means that the organic−fullerene blend is not ideal for durable devices. Among alternative electron acceptors are inorganic nanocrystalline materials, such as metal oxides[2] and chalcogenides,[3] which may be dispersed in solution together with the organic donor, or deposited as rigid nanostructures which may be filled with the organic donor material. External quantum efficiencies of over 40% have been achieved in photovoltaic devices based on conjugated polymers combined with metal oxide nanoparticles or nanoparticle films in these ways.[2,4] However, the overall performance of such devices is disappointing, and is apparently limited by both charge transport and charge separation efficiency. A key advantage of using metal oxides as electron acceptors is the capability to produce rigid, nanocrystalline structures that present a direct and ordered path for photogenerated electrons to the collecting electrode. This may be done by using templated porous structures,[5] tetrapods,[6] or vertically aligned nanorods. Zinc oxide (ZnO) is of interest on account of its high electron mobility,[7] the availability of low-temperature synthesis, and the potential for controlling the morphology through simple processing from solution. ZnO nanorods grown perpendicular to the substrate[8] are particularly interesting. Recently, the first successful attempts to replace TiO_2 nanoparticle films with ZnO nanorods in solid-state dye sensitized solar cells[9] and inorganic bulk heterojunctions[10] have been reported. In both cases, the promising performance of the devices based on ZnO nanorods is attributed in part to the ease of electron transport and collection.

In this paper, we report on the photovoltaic performance of nanocrystalline ZnO:P3HT polymer structures consisting of either vertically aligned ZnO nanorods or randomly oriented ZnO nanoparticles. Our strategy was to grow ZnO nanorods perpendicular to a dense ZnO "backing layer" and fill the structure with polymer. An amphiphilic molecular interface layer was used to optimize interfacial electron transfer between the polymer and the ZnO nanostructure. Through a comparison of device performance, charge recombination, and charge transport behavior, we demonstrate that the use of nanorods instead of nanoparticles and the use of an amphiphilic molecular interface layer both result in significant improvements in device performance, and that these improvements are due in part to slower charge recombination.

* Address correspondence to this author. E-mail: jenny.nelson@imperial.ac.uk. Fax: +44-207-581-3817. Phone: +44-207-594-7581.
† Department of Physics, Imperial College London.
‡ University of Jaffna.
§ Department of Chemistry, Imperial College London.
⊥ École Polytechnique Fédérale de Lausanne.

10.1021/jp0571372 CCC: $30.25
Published on Web 03/31/2006

Materials and Methods

Sample Preparation. Samples were prepared on indium tin oxide coated glass substrates (ITO, ~1 cm^2, 10−15 Ω/square), which were first cleaned by ultrasonic agitation in acetone and 2-propanol. The cleaned substrates were then covered with a dense ZnO layer, to prevent direct contact of the polymer with ITO. The dense films were prepared by spray pyrolysis at 400 °C. The precursor solution contained zinc acetate (1.756 g) dissolved in 20 mL of methanol. After deposition, the films were calcined at 400 °C for 20 min, resulting in ZnO films of thickness about 50 nm. Porous ZnO nanoparticle films were deposited onto the dense films by spin-coating diluted ZnO paste, prepared by the methods described in ref 11.

ZnO rods were prepared onto ZnO dense films, following the method described in ref 8. Briefly, a stock solution of $ZnSO_4 \cdot 7H_2O$ (0.02 M) and NH_4Cl (0.6 M) was prepared with H_2O as a solvent. This solution was further diluted to 0.01 M in Zn^{2+} and then the pH was adjusted to 11.00 with NaOH. ZnO rod deposition onto the ZnO dense layers took place at 60 °C for 3−6 h. Following deposition, substrates were rinsed and sonicated in distilled water, and finally dried under nitrogen flow.

Poly(3-hexylthiophene) polymer (P3HT) was used as the hole transporting and light absorbing material. First, the metal oxide films were immersed overnight either in a solution of polymer in chlorobenzene (~2 mg/mL) or in a 0.3 mM solution of amphiphilic polypyridyl ruthenium complex, *cis*-RuLL′$(SCN)_2$ (L = 4,4′-dicarboxylic acid-2,2′-bipyridine, L′ = 4,4′-dinonyl-2,2′-bipyridine) (Z907) in acetonitrile:*tert*-butyl alcohol (1:1 vol %) at 100 °C. The dip-coated film was then "wiped" by a quick blow with dry nitrogen gas and heated at 50 °C in air. Finally, an 80 nm polymer layer was deposited onto the films by spin-coating from a polymer solution in chlorobenzene (15−20 mg/mL) at 2000 rpm.

Sample Characterization. Transient absorption and photovoltaic device measurements were undertaken as reported previously.[12] Transient absorption studies employed low excitation density (540 nm excitation, <1 ns pulse duration, 0.8 Hz, intensity ~30 μJ/pulse/cm^2). For photovoltaic devices, a layer of poly(ethylenedioxythiophene) (PEDOT) doped with poly(styrenesulfonic acid) (PSS) was deposited by spin coating[4] on top of the spin-coated polymer layer before evaporation of a Au top contact. The active area of each device was ~4.2 mm^2. Current−voltage measurements were obtained with a ScienceTech solar simulator and AM 1.5 spectral filter. The light intensity was calibrated by using band-pass filters of known transmission combined with a silicon photodiode with independently certified spectral response. The lamp intensity was adjusted to give close (±10%) agreement with the theoretical one-sun AM 1.5 intensity over the spectral region of the polymer optical absorption (400−700 nm).

Results and Discussion

Figure 1a−c shows typical scanning electron micrographs (SEM) of single-crystal ZnO rods and ZnO particles deposited on a dense ZnO underlayer. The ZnO particles have sizes in the range of 70 to 150 nm. The rods stand almost perpendicular to the substrate, have a similar diameter, in the range 60 to 100 nm, and are about 0.5−1.0 μm long, yielding a roughness factor, defined as the ratio of microscopic surface area of the film to the area of substrate covered, for both film types of the order of 10. We study films of similar thickness (~0.5 μm) for both nanorod and nanoparticle films. The dimensions of the rods are too large for efficient photoinduced charge separation, because the typical pore diameter (similar to the ZnO rod diameter at ~100 nm) is larger than the polymer exciton diffusion length (<10 nm) and therefore the majority of photogenerated excitons are likely to recombine before reaching the polymer/ZnO interface for dissociation. Previous studies have shown that the effective exciton diffusion length in thiophene polymer/TiO_2 hybrid structures is less than 10 nm and that complete charge separation is not achieved even with pore diameters of ~20 nm.[12,13] The films are also rather thick compared to TiO_2 structures studied previously and may impede efficient charge collection. However, the similar dimensions of rods and particles enabled us to focus on the effect of morphology, despite the suboptimal photoinduced charge generation in both cases. We found that the dimension of the grown rods is highly dependent on reaction time and the quality of the dense layer. We will report on the influence of the aspect ratio of the ZnO nanorods on charge recombination and device performance elsewhere.[14]

In this study, we use regioregular poly(3-hexylthiophene) (P3HT) as the light-absorbing and hole-transporting component of the device. Our previous studies of polymer/TiO_2 nanoparticle films have demonstrated that device performance improves by dip-coating the TiO_2 film in a dilute polymer solution prior to spin-coating the polymer material.[12,13] In this study, we extend this approach to the use of an amphiphilic dye *cis*-RuLL′$(SCN)_2$ (L = 4,4′-dicarboxylic acid-2,2′-bipyridine, L′ = 4,4′-dinonyl-2,2′- bipyridine) (Figure 1d), referred to as Z907, for the dip-coating step. Our rationale is 2-fold: first, that the amphiphilic dye should improve the wetting of the oxide surface by the polymer, and second, that the dye should assist interfacial electron transfer from the polymer to the ZnO conduction band. The ZnO films (either particles or rods) were first dipped in a dilute solution of either the Z907 dye or, as a control, P3HT polymer, before a layer of P3HT polymer (effective thickness 80 nm) was spin-coated on top. Dip-coating in the dye solution did not result in a significant coloration of the film, as expected for monolayer dye coverage of these rather low roughness factor films. Following deposition of the spin-coated layer, the absorption spectra of the composite films corresponded closely to that of P3HT absorption alone, with the control P3HT dip- and spin-coated film (ZnO/$P3HT^d$/$P3HT^s$) showing approximately 25% higher overall optical density, compared to the dye-treated films (ZnO/$Z907^d$/$P3HT^s$), where superscripts "d" and "s" refer to dip-coated and spin-coated layers, respectively (see Figure 3b, inset). Polymer/ZnO films based on ZnO particles showed 13% higher optical density relative to those based on ZnO nanorods. Expected energy levels for the polaron states of ZnO, Z907, and P3HT, determined from literature values,[12,15,16] are shown in Figure 1e. The LUMO of Z907 is lower in energy than that of P3HT, enabling an electron transfer cascade from P3HT to the Z907 interface layer to ZnO and, thereby, potentially enhancing charge separation at the ZnO interface. Additionally, on account of the deep HOMO level of Z907 relative to P3HT, the Z907 layer is expected to obstruct hole transfer between P3HT and metal oxide, and thus to localize hole-polarons in the P3HT away from the metal oxide surface.

The photoinduced electron-transfer yield and charge recombination kinetics in the composite films were monitored by μs−ms transient absorption spectroscopy. Figure 2 compares the photoinduced change in absorbance, ΔOD, at a probe wavelength of 900 nm (corresponding to the absorption maximum of $P3HT^+$ polarons), for ZnO rod/$Z907^d$/$P3HT^s$ films, ZnO particle/$Z907^d$/$P3HT^s$ films, and ZnO rod/$P3HT^d$/$P3HT^s$ films, following excitation at the P3HT absorption maximum (540 nm). No photoinduced absorption signal was observed in either dye-

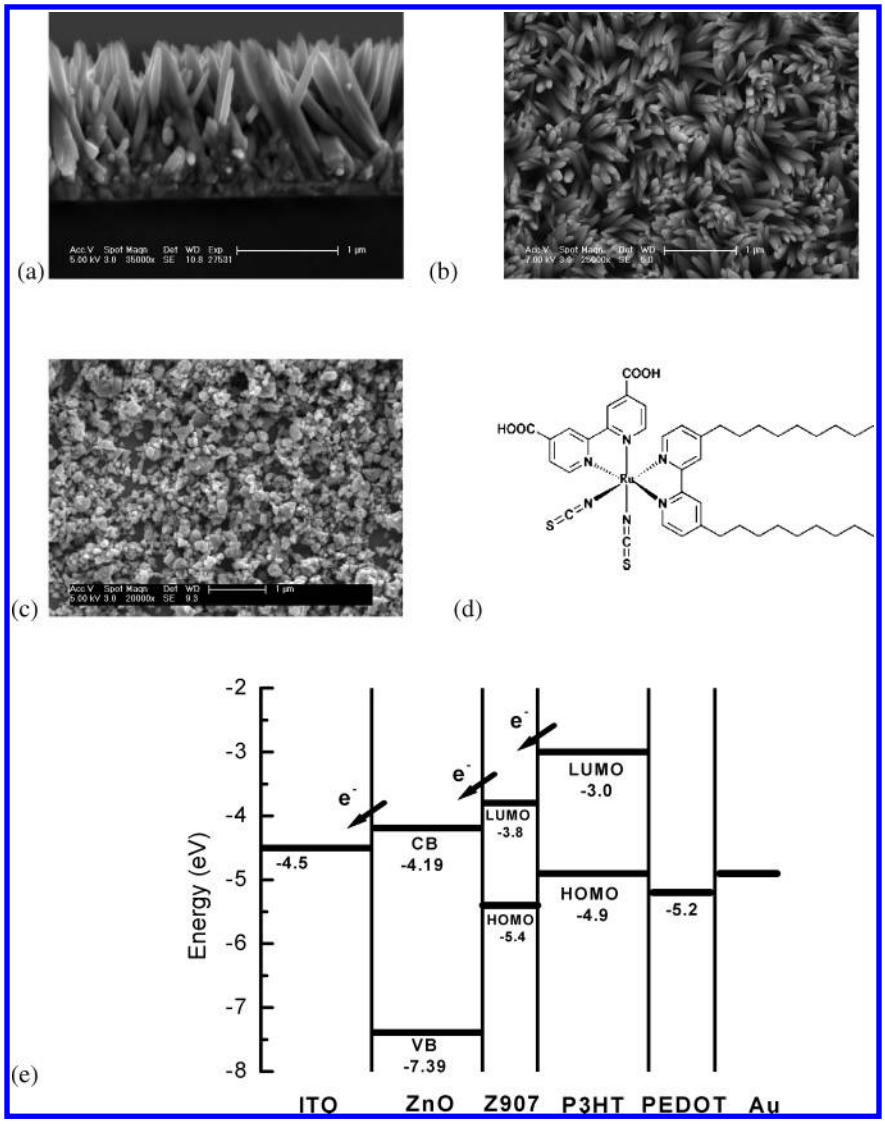

Figure 1. (a−c) SEM micrographs of ZnO nanorod and nanoparticle films grown on dense ZnO backing layers on an ITO substrate: (a) cross-sectional view and (b) top view of ZnO rods and (c) top view of ZnO particle films. (d) Chemical structure of the dye Z907. (e) Schematic energy level diagram of the ITO/ZnO/Z907^{d}/P3HT^{s}/PEDOT:PSS/Au device polymer device (where superscripts "d" and "s" refer to dip-coated and spin-coated layers, respectively) showing electron-transfer pathways. Numbers represent energies in eV relative to the vacuum level.

treated structure at the probe wavelength of the Z907 dye (700 nm) or in pristine P3HT polymer films at the probe wavelength of 900 nm. Therefore, the observed signal for the composite films on the 1 μs−100 ms time scale can safely be assigned to photoinduced hole-polarons in the P3HT, rather than to dye cation states or triplet states of P3HT. The figure shows that the lifetime of hole polarons on the dye-treated ZnO rod/Z907^{d}/P3HT^{s} structure is remarkably long (∼6 ms) and is approximately 2 orders of magnitude longer than that for the equivalent structure made with particles. In addition, Figure 2 shows that dye treatment improves the charge-transfer yield of ZnO rod:P3HT structures by at least 50% relative to the P3HT treated control (noting that the ground-state absorbance is lower for the dye-treated structure). (The yield is defined from the change in absorbance at 1 μs, neglecting any possible contributions from geminate recombination on time scales too fast for detection.) Moreover, the half-life for the dye-coated rods is slower by a factor of 4−5 than that for the uncoated rods.

The slower recombination kinetics observed for rods compared to particles may result from several factors. The most likely reason is that the better connectivity of the rods leads to easier escape for electrons from interfacial recombination sites.

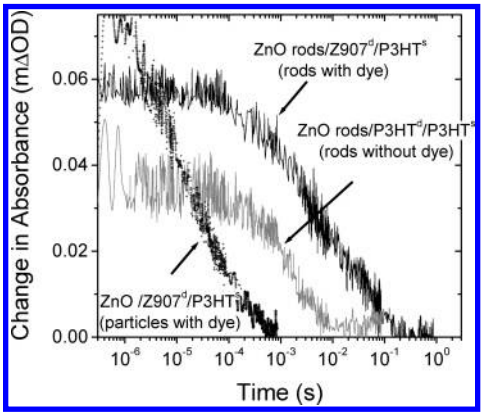

Figure 2. Photoinduced change in absorbance for structures consisting of dye-treated ZnO rod/Z907^{d}/P3HT^{s} (solid black line), dye-treated ZnO particle/Z907^{d}/P3HT^{s} (black crosses), and P3HT-treated ZnO rod/P3HT^{d}/P3HT^{s} (gray line). In each case, the ZnO nanocrystal film is ∼550 nm thick and is deposited on 50 nm of dense ZnO on an ITO coated glass substrate. The excitation density is ∼30 μJ/pulse/cm^2 (corresponding to 1.3×10^{14} incident photons/pulse/cm^2) at 540 nm and all the samples are excited through the substrate side.

It is known from modeling studies of charge recombination in nanoparticle films that improved connectivity between nanoparticles can lead to slower recombination by 2 orders of magnitude at low excitation densities.[17] Additional influences on the recombination kinetics include differences in the surface structure of nanoparticles and nanorods, influencing the density and nature of surface traps. The influence of ZnO rod morphology on recombination kinetics will be the subject of a separate study.

The improved charge separation yield observed with the Z907 layer may be attributed to two mechanisms. First, the energy level structure at the ZnO/Z907^d/P3HT^s interface, illustrated in Figure 1e, enables electron cascade from P3HT to ZnO while blocking hole transfer, thus improving charge separation, as mentioned previously. (We note that this cascade could also function by exciton energy transfer from the P3HT to the Z907 dye layer, followed by electron injection into the ZnO and back hole transfer into the P3HT.) Second, the amphiphilic dye is expected to orient such that its polar side groups attach to the oxide surface while the nonpolar side chains are directed to the interior of the pores. This nonpolar surface is expected to be more easily wetted by the conjugated polymer than the bare, polar ZnO.[16] The slower recombination dynamics observed for the Z907-treated film are consistent with the function of the Z907 layer as a hole blocking layer, increasing the spatial separation of photogenerated electrons and holes after charge separation. Since charge separation is more efficient with the dye layer present, one could expect the charge recombination rate to be increased by the dye, assuming that the same donor−acceptor interaction controls both processes. However, in this system we believe that charge separation is a multiple step process involving electron and/or exciton transfer to the dye as an intermediate, thereby allowing rapid charge separation across this multilayer interface, while charge recombination requires direct charge transfer from ZnO to P3HT, with the increased spatial separation of these layers retarding charge recombination. In cases such as this, faster charge injection does not necessarily require faster recombination.

Photovoltaic devices were fabricated by spin-coating a layer (effective thickness 50 nm) of poly(ethylenedioxythiophene)/polystyrene sulfonate, PEDOT:PSS, before thermal evaporation of Au top contacts onto a ZnO rod or particle structure that had previously been dip-treated in either Z907 or P3HT and spin-coated with P3HT (effective thickness 80 nm). In all cases, the substrate consisted of a 50 nm dense ZnO layer on ITO coated glass. The highly conductive PEDOT:PSS layer is intended to keep series resistance low and to reduce surface roughness by helping to fill the voids in the films. Inspection of the electrodes on structures with and without a PEDOT:PSS layer present confirms that the PEDOT:PSS layer improves the smoothness of the top surface and the electrode quality. When the effective thickness of the P3HT polymer layer was increased beyond 80 nm, the short circuit current density of the device was decreased. This effect is attributed to increased series resistance by the thicker polymer layer, in accordance with previous studies with nanocrystalline TiO_2 films.[12,18]

Good device performance depends on having suitable asymmetric electron and hole collecting contacts to minimize shunt paths. To this end, we endeavored to optimize the ZnO dense layer so that direct contact between P3HT (HOMO level ~4.9 eV) and ITO (work function ~4.7 eV, as measured by Kelvin probe) was minimized. It should be noted that dense TiO_2 could not be used as, although it provides a more effective hole-blocking layer than dense ZnO, it also presents a barrier to electron transport from ZnO into ITO and thereby limits photocurrent collection. The PEDOT:PSS layer helped to reduce shunt losses through direct contact between ZnO rods or particles and the metal top contact, and thus acts as an electron blocking layer. The Z907 dye layer also appeared to reduce shunt losses, as discussed below. Devices without either dye layer or PEDOT:PSS showed large leakage currents and very low V_{oc}.

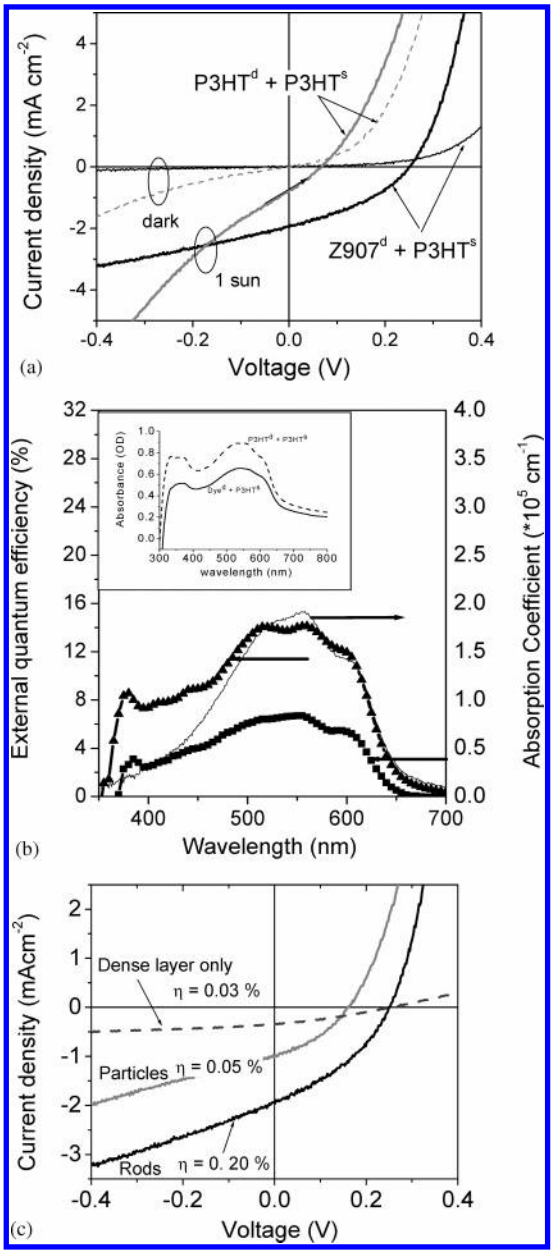

Figure 3. (a) Current−voltage characteristics of ZnO rod:P3HT devices with (black lines) and without (gray lines) a Z907 dye layer under simulated AM1.5 solar irradiation (100 mW cm^{-2}) (solid lines) and in the dark (dashed lines). (b) External quantum efficiency spectra of ZnO rod:P3HT devices with (triangles) and without (squares) dye treatment. The absorption spectrum of the P3HT polymer (solid line) is shown for comparison. The inset shows the optical density of similar structures without a top contact, with dye (solid line) and without dye (dashed line). Notice that the dye does not increase absorbance. (c) ZnO:P3HT devices with different morphology (rods, particles, and dense layer only) under 1 sun (100 mW cm^{-2}). The device structure is ITO/dense ZnO (50 nm)/ZnO (~550 nm)/Dye^d/P3HT^s/PEDOT:PSS/Au in the case of the rod and particle devices, and ITO/dense ZnO (50 nm)/Dye^d/P3HT^s/PEDOT:PSS/Au for the dense layer only device.

Figure 3a shows the effect of dye treatment on the current density−voltage ($J-V$) characteristics of ZnO rod:P3HT de-

vices. The figure shows that dye treatment suppresses the dark current and increases both open circuit voltage (V_{oc}) and short circuit current density (J_{sc}) under simulated solar irradiation, relative to the case where the nanorods are dip-coated in P3HT. The increased V_{oc} is attributed to the action of the dye layer both in blocking holes in the P3HT from reaching the ZnO surface and recombining with electrons in the oxide (which is consistent with the slower recombination dynamics observed in the transient absorption studies), and in blocking direct contact between P3HT and ITO through defects in the imperfect ZnO dense layer. Although the P3HT only device shown in Figure 3a suffers from a large shunting effect, this was not anomalous. Similar shunt losses were observed for all other devices prepared by dip-coating in P3HT instead of dye treatment. The increased photogeneration yield in the presence of the dye may be attributed to improved wetting of the oxide surface by the polymer in the presence of the amphiphilic dye, leading to an increase in the interfacial area available for photoinduced charge separation. These ideas are supported by the observation that an alternative, nonamphiphilic dye showed similar function in suppressing dark current but did not improve photocurrent. We stress that the optical density of the Z907 dye layer is negligible (Figure 3b, inset) and, therefore, the dye layer does not contribute significantly to light harvesting.

Figure 3b shows the external quantum efficiency (EQE) spectra of ZnO rod:P3HT devices with and without dye treatment. The inset shows the optical density of the corresponding films without top electrodes. The similar shape of the EQE spectra for both devices, following the absorption spectrum of the P3HT polymer, confirms that there is no contribution from the dye to photocurrent generation in the device. The dye layer, however, improves peak external quantum efficiency of the device from 7% to over 14% at 550 nm, despite a reduced optical absorbance. This is consistent with the increased polaron generation yield observed in the transient absorption studies. Integrating the product of the measured EQE with the photon flux density of the AM1.5 solar spectrum yields a short circuit current density of $\sim$1.8 mA cm^{-2} for the dye-treated ZnO rod:P3HT device, which is consistent, within experimental uncertainties, with the measured J_{sc} under AM1.5 conditions of 2.0 mA cm^{-2}.

Figure 3c shows the effect of ZnO layer morphology on the current−voltage characteristics of dye-treated ZnO:P3HT devices. Introducing ZnO nanorods or particles increases J_{sc} compared to bilayer devices made with P3HT on dense ZnO layer, as expected due to the increased interfacial area. Moreover, devices made with nanorods show higher V_{oc} and J_{sc} than similar devices made with nanoparticles, resulting in a power conversion efficiency over four times greater than that for similar devices made with nanoparticles. The higher V_{oc} and J_{sc} are consistent with the slower recombination in rod than particle based structures, noted above. The higher J_{sc} is also consistent with high electron mobilities observed in ZnO nanorods.[7,9] Additionally, some influence of pore geometry on P3HT chain alignment and, hence, on hole transport, as reported elsewhere,[19] cannot be ruled out. In all cases the V_{oc} values are rather small, but are consistent with the limit of $\sim$0.5−0.7 eV obtained from the difference between the conduction band edge of the ZnO, estimated to lie at 4.2−4.4 eV below vacuum level, and the HOMO of the polymer.

In conclusion, we find the charge recombination in the structure containing vertically aligned ZnO nanorods treated with an amphiphilic molecular interface layer is remarkably slow, with a half-life of $\sim$6 ms, over 2 orders of magnitude slower than that for similar structures based on randomly oriented ZnO nanoparticles. A photovoltaic device based on the nanorod structure with P3HT polymer shows power conversion efficiency over four times greater than that for a similar device based on nanoparticles. The best ZnO nanorod:P3HT device using the molecular interface layer yields a short circuit current density of 2 mA cm^{-2} under AM1.5 illumination (100 mW cm^{-2}) and peak external quantum efficiency over 14%, resulting in a power conversion efficiency of 0.2%. There were six devices per substrate and the variation in efficiencies of the working devices was within 15%. Although the reported current densities here are greater than most previously published values for TiO_2/polymer solar cells, the J_{sc} and V_{oc} values are both significantly lower than those for the best polymer−fullerene solar cells. The low V_{oc} can be attributed partly to shunt losses due to imperfections of the dense ZnO layer, and the low J_{sc} to low charge separation efficiency due to the large film pore sizes ($\sim$100 nm) relative to the P3HT exciton diffusion length. Improved performance can be expected through optimizing the dimensions of the ZnO rods and improving the blocking function of the dense ZnO layer.

Acknowledgment. We thank Merck Chemicals Ltd. for providing the P3HT polymer used in this study. We acknowledge the Commission of the European Community (Project MOLYCELL Contract No. 502783) for their financial assistance. A.M.P. acknowledges the Spanish Secretaría de Estado de Universidades e Investigación del Ministerio de Educación y Ciencia for a postdoctoral fellowship. We would like to thank Dr. Jessica E. Kroeze for assistance in TAS data treatment and Dr. Brian O'Regan for useful discussions.

References and Notes

(1) Ma, W.; Yang, C.; Gong, X.; Lee, K.; Heeger, A. J. *Adv. Funct. Mater.* **2005**, *15*, 1617. Reyes-Reyes, M.; Kim, K.; Carrol, D. L. *Appl. Phys. Lett.* **2005**, 083506. Kim, Y.; Cook, S.; Tuladhar, S. M.; Choulis, S. A.; Nelson, J.; Durrant, J. R.; Bradley, D. D. C.; Giles, M.; McCulloch, I.; Ha, C. S.; Ree, M. *Nat. Mater.* **2006**. In press.

(2) Beek, W. J. E.; Wienk, M. M.; Janssen, R. A. J. *Adv. Mater.* **2004**, *16*, 1009.

(3) Huynh, W. U.; Dittmer, J. J.; Libby, W. C.; Whiting, G. L.; Alivisatos, A. P. *Adv. Funct. Mater.* **2003**, *13*, 73.

(4) Ravirajan, P.; Haque, S. A.; Durrant, J. R.; Smit, H. J. P.; Kroon, J. M.; Bradley, D. D. C.; Nelson, J. *Appl. Phys. Lett.* **2005**, *86*, 143101.

(5) (a) Coakley, K. M.; McGehee, M. D. *Appl. Phys. Lett.* **2003**, *83*, 3380. (b) Zukalova, M.; Zukal, A.; Kavan, L.; Nazeeruddin, M. K.; Liska, P.; Gratzel, M. *Nano Lett.* **2005**, *5*, 1789.

(6) Sun, B.; Snaith, H. J.; Dhoot, A. S.; Westenhoff, S.; Greenham, N. C. *J. Appl. Phys.* **2005**, *97*, 014914.

(7) Makino, T.; Segawa, Y.; Tsukazaki, A.; Ohtomo, A.; Kawasaki, M. *Condensed. Matter* **2005**, *1*−*4*, 0507009.

(8) Yamabi, S.; Imai, H. *J. Mater. Chem.* **2002**, *12*, 3773.

(9) Law, M.; Greene, L. E.; Johnson, J. C.; Saykally, R.; Yang, P. *Nat. Mater.* **2005**, *4*, 455.

(10) Lévy-Clément, C.; Tena-Zaera, R.; Ryan, M. A.; Katty, A.; Hodes, G. *Adv. Mater.* **2005**, *17*, 1512.

(11) (a) Westermark, K.; Rensmo, H.; Siegbahn, H.; Keis, K.; Hagfeldt, A.; Ojamae, L.; Persson, P. *J. Phys. Chem. B* **2002**, *106*, 10102. (b) Kavan, L.; O'Regan, B.; Gratzel, M. J. *J. Electroanal. Chem.* **1993**, *346*, 291.

(12) Ravirajan, P.; Haque, S. A.; Durrant, J. R.; Poplavskyy, D.; Bradley, D. D. C.; Nelson, J. *J. Appl. Phys.* **2004**, *95*, 1473.

(13) Ravirajan, P.; Haque, S. A.; Durrant, J. R.; Bradley, D. D. C.; Nelson, J. *Adv. Funct. Mater.* **2005**, *15*, 609.

(14) Peiró, A. M.; Ravirajan, P.; Govender, K.; Smyth-Boyle, D.; O'Brien, P.; Bradley, D. D. C.; Nelson, J.; Durrant, J. R. *J. Mater. Chem.*, in press.

(15) (a) Chiguvare, Z.; Dyakonov, V. *Phys. Rev. B* **2004**, *70*, 235207. (b) Linsebigler, A. L.; Lu, G.; Yates, J. T., Jr. *Chem. Rev.* **1995**, *95*, 735. (c) Xu, Y.; Schoonen, M. A. A. *Am. Mineral.* **2000**, *85*, 543.

(16) Schmidt-Mende, L.; Zakeeruddin, S. M.; Gratzel, M. *Appl. Phys. Lett.* **2005**, *86*, 013504.

(17) Nelson, J.; Chandler, R. E. *Coord. Chem. Rev.* **2004**, *248*, 1181.

(18) Nelson, J.; Kirkpatrick, J.; Ravirajan, P. *Phys. Rev. B* **2004**, *69*, 035337.

(19) Liu, Y.; Coakley, K. M.; McGehee, M. D. *Proc. SPIE Int. Soc. Opt. Eng.* **2004**, *5215*, 187.